Available online at www.sciencedirect.com
ScienceDirect
Procedia Computer Science 1 (2010) 1915–1923
Procedia Computer Science
www.elsevier.com/locate/procedia

International Conference on Computational Science, ICCS 2010

A mimetic tensor artificial viscosity method for arbitrary polyhedral meshes☆

Konstantin Lipnikov[1,*], Mikhail Shashkov[1]

[a]*Applied Mathematics and Plasma Physics Group, Los Alamos National Laboratory, MS B284, Los Alamos, NM 87545, USA*

Abstract

We construct a new mimetic tensor artificial viscosity on general polyhedral meshes. The tensor viscosity is designed as a discretization of the differential operator div ($\mu\nabla\mathbf{u}$) with the full fourth-order tensor μ. We demonstrate performance of the new artificial viscosity on a set of test problems.

Keywords: mimetic finite differences, Lagrangian hydrodynamics, artificial viscosity

1. Introduction

We consider a system of hydrodynamic equations in Lagrangian coordinates describing motion of a compressible gas [1]:

$$\begin{aligned} \frac{1}{\rho}\frac{D\rho}{Dt} &= -\operatorname{div}\mathbf{u}, \\ \rho\frac{D\mathbf{u}}{Dt} &= -\nabla \mathrm{p}, \\ \rho\frac{D\varepsilon}{Dt} &= -\mathrm{p}\operatorname{div}\mathbf{u}, \end{aligned} \tag{1}$$

where ρ, p, $\mathbf{u}$ and ε are the gas density, pressure, velocity and internal energy, respectively, and D/Dt denotes the material derivative. The system of three equations has four unknowns; therefore, it is closed by an equation of state.

These equations come from three fundamental conservations laws for the mass, momentum, and energy. The aim of any compatible (mimetic) discretization method is to develop a system of discrete equations that has three discrete conservations laws. For a staggered discretization [2] considered here, the discrete velocity unknowns are defined at mesh points (three numbers per point), while the discrete pressure, density and internal energy are defined on mesh elements (one number per element).

☆This work was carried out under the auspices of the National Nuclear Security Administration of the U.S. Department of Energy at Los Alamos National Laboratory under Contract No. DE-AC52-06NA25396 and the DOE Office of Science Advanced Scientific Computing Research (ASCR) Program in Applied Mathematics Research.
*The corresponding author
Email addresses: lipnikov@lanl.gov (Konstantin Lipnikov), shashkov@lanl.gov (Mikhail Shashkov)
URL: math.lanl.gov/~lipnikov (Konstantin Lipnikov), cnls.lanl.gov/~shashkov (Mikhail Shashkov)

1877-0509
doi:10.1016/j.procs.2010.04.215

Modeling of high-speed flows with shocks using the staggered discretization requires introduction of an *artificial numerical viscosity* [3, 4, 5]. This viscosity stabilizes the simulation by spreading the shock across a few mesh elements. The basic requirements for design of the artificial viscosity, as well as overview of existing methods, can be found in [6, 4]. In this paper, we extend the Tensor Artificial Viscosity (TAV) method developed in [7] for two-dimensional problems to three dimensions.

The TAV proposed originally in [8] is designed as a discretization of the differential operator $\mathrm{div}\,(\mu\nabla\mathbf{u})$. The method in [8] is limited to the case of a scalar coefficient μ and polygonal meshes with convex elements. In the recent paper [9], the authors derived a high-order discretization for the tensor viscosity using the finite-element technique. For quadrilateral meshes, they showed that the finite element method with the reduced quadrature rule reproduces the mimetic formulation. A connection between two methods has been also proved in [10] for diffusion problems. To some extend, the mimetic method can be considered as a natural extension of the finite element technique to general meshes. In [9], the authors considered only non-degenerate quadrilateral and non-degenerate hexahedral meshes and again only a scalar μ. The aforementioned limitations were removed in [7] for two-dimensional problems in both the Cartesian (x-y) and axisymmetric (r-z) coordinate systems.

One of the important features of the TAV is its ability to act only in the direction of a shock by exploiting the flexibility provided by the full tensor μ. Design of the appropriate fourth-order tensor μ is the active research area. Derivation of the mimetic discretization of the three-dimensional operator $\mathrm{div}\,(\mu\nabla\mathbf{u})$ with the full tensor coefficient μ on a general polyhedral mesh, which is developed in this paper, is the foundation for future developments. This discretization follows the new mimetic technology developed in [11, 12] for diffusion problems.

The paper outline is as follows. In Section 2, we describe a continuous analog of the TAV and recall how it enters the equations of Lagrangian hydrodynamics. In Section 3, we develop the three-dimensional TAV method. A few two-dimensional and three-dimensional experiments are presented in Section 4.

2. Artificial viscosity

For shock calculations, an artificial numerical viscosity has to be added to the discrete momentum equation. Being artificial, the viscosity stress tensor does not need to be symmetric. Following [8, 9], we define the artificial viscosity as an approximation of the elliptic operator:

$$\mathbf{f}^{vis} = \mathrm{div}\,(\mu\nabla\mathbf{u}). \tag{2}$$

where, contrary to [8, 9], we allow μ be a *full fourth-order* tensor. The continuous forms of the modified momentum and internal energy equations are

$$\rho\frac{D\mathbf{u}}{Dt} = -\nabla\mathrm{p} + \mathrm{div}\,(\mu\nabla\mathbf{u}), \qquad \rho\frac{D\varepsilon}{Dt} = -\mathrm{p}\,\mathrm{div}\,\mathbf{u} + (\mu\,\nabla\,\mathbf{u}) : \nabla\,\mathbf{u}.$$

The symbol ':' means the dot product of two tensors.

3. Mimetic tensor artificial viscosity method

We refer to [7] for a detailed derivation of semi-discrete equations and focus our attention on an approximation of the last term in the modified momentum equation. Contrary to [7], the current derivation follows the finite element framework to illustrate a close connection between the mimetic finite difference and finite element methods.

Let $\mathcal{T}_h$ be a partition of the computation domain into non-overlapping polyhedral elements E. This partition may contain non-convex and degenerate (two adjoin faces are parallel) elements. We denote the volume of E by $|E|$, the area of its face f by $|f|$, the position vector of its vertex v by $\mathbf{x}_v$. Let h be the characteristic mesh size, the diameter of the largest polyhedron.

We consider a staggered discretization. The degrees of freedom for the velocity are defined at mesh points. For a smooth function $\mathbf{v}$, we define the global vector $\mathbf{V}$ of degrees of freedom. The size of $\mathbf{V}$ is triple the number of mesh points. We also need the restriction of this vector to element E that we denote by $\mathbf{V}_E$. Similarly, $\mathbf{V}_{E,v}$ denotes the restriction of $\mathbf{V}_E$ to vertex v of E. This is a three-dimensional vector. Finally, let $n_{E,v}$ be the size of vector $\mathbf{V}_E$, i.e. triple the number of vertices in E.

Multiplying both sides of (2) by a test function $\mathbf{v}$ and integrating by parts, we get

$$\int_\Omega \mathbf{f}^{vis} \cdot \mathbf{v} \, \mathrm{d}V = -\int_\Omega (\mu \nabla \mathbf{u}) : \nabla \mathbf{v} \, \mathrm{d}V + \int_{\partial\Omega} ((\mu \nabla \mathbf{u}) \cdot \mathbf{n}) \cdot \mathbf{v} \, \mathrm{d}S,$$

where $\mathbf{n}$ is the exterior normal vector. For clarity, we assume that the boundary conditions are such that the last integral is zero. We apply accurate quadrature rules to the other integrals. Each rule is written as a vector-matrix-vector multiplication with vectors of degrees of freedom and an appropriate matrix, for instance:

$$\int_\Omega \mathbf{f}^{vis} \cdot \mathbf{v} \, \mathrm{d}V = (\mathbf{F}^{vis})^T \, \mathbf{M} \, \mathbf{V} + O(h),$$

where the $\mathbf{F}^{vis}$ is the global vector of point-based degrees of freedom of the vector function $\mathbf{f}^{vis}$. The $O(h)$ term must be small for sufficiently smooth functions $\mathbf{f}^{vis}$ and $\mathbf{v}$. Similarly, the other quadrature gives

$$\int_\Omega (\mu \nabla \mathbf{u}) : \nabla \mathbf{v} \, \mathrm{d}V = \mathbf{U}^T \, \mathbf{A} \, \mathbf{V} + O(h). \tag{3}$$

Given matrices $\mathbf{M}$ and $\mathbf{A}$, we obtain the desired viscous forces at mesh points:

$$\mathbf{F}^{vis} = -\mathbf{M}^{-1} \mathbf{A} \, \mathbf{U}.$$

Note that the actual computations require only the vector $\mathbf{M}\,\mathbf{F}^{vis}$. As in the finite element framework, both matrices are assembled from local elemental matrices:

$$\mathbf{M} = \sum_{E \in \mathcal{T}_h} \mathbf{N}_E \mathbf{M}_E \mathbf{N}_E^T, \qquad \mathbf{A} = \sum_{E \in \mathcal{T}_h} \mathbf{N}_E \mathbf{A}_E \mathbf{N}_E^T,$$

where $\mathbf{N}_E$ is the assembling matrix with only zero and one entries. Clearly to guarantee (3), the elemental matrices must also provide accurate quadrature rules:

$$\int_E \mathbf{f}^{vis} \cdot \mathbf{v} \, \mathrm{d}V = (\mathbf{F}_E^{vis})^T \, \mathbf{M}_E \, \mathbf{V}_E + |E| \, O(h), \qquad \int_E (\mu \nabla \mathbf{u}) : \nabla \mathbf{v} \, \mathrm{d}V = \mathbf{U}_E^T \, \mathbf{A}_E \, \mathbf{V}_E + |E| \, O(h). \tag{4}$$

The first quadrature in (4) is trivial: the matrix $\mathbf{M}_E$ is diagonal with equal entries $|E|/n_{E,v}$. This quadrature rule is exact for constant functions. To derive the second quadrature, we recall a few facts from linear algebra.

Let $\mathbf{B}_E$ be a full rank $n_{E,v} \times n_{E,v}$ matrix, representing a change of the basis in the linear space $\Re^{n_{E,v}}$. The columns of $\mathbf{B}_E$ are the new basis vectors. Change of the basis induces the following congruent transformation of the matrix $\mathbf{A}_E$:

$$\hat{\mathbf{A}}_E = \mathbf{B}_E^T \, \mathbf{A}_E \, \mathbf{B}_E. \tag{5}$$

If somebody gives us the basis vectors and the matrix $\hat{\mathbf{A}}_E$, we calculate immediately the matrix $\mathbf{A}_E$ using (5). Unfortunately, the reality is that only a partial information about the basis and the matrix $\hat{\mathbf{A}}_E$ is available *a priory*. Assume that (a) we know m basis vectors $\mathbf{B}_i$, $i = 1, \ldots, m$ and (b) we can calculate somehow m vectors $\mathbf{R}_i = \mathbf{A}_E \mathbf{B}_i$ without using the matrix $\mathbf{A}_E$. Then, it is possible to complete the basis in such a way that the matrix $\hat{\mathbf{A}}_E$ is block-diagonal.

Lemma 3.1. *Let m basis vectors $\mathbf{B}_i$ be given. Furthermore, let the vectors $\mathbf{R}_i = \mathbf{A}_E \mathbf{B}_i$, $i = 1, \ldots, m$, be given. Let us complete the basis by vectors $\mathbf{B}_j$, $j = m+1, \ldots, n_{E,v}$, such that*

$$\mathbf{B}_j^T \, \mathbf{R}_i = 0, \qquad 1 \le i \le m < j \le n_{E,v}. \tag{6}$$

Then, we have the following identity:

$$\mathbf{B}_E^T \, \mathbf{A}_E \, \mathbf{B}_E = \begin{bmatrix} \hat{\mathbf{A}}_E^1 & 0 \\ 0 & \hat{\mathbf{A}}_E^2 \end{bmatrix}.$$

Proof. The proof is straightforward. By assumption, $\mathbf{B}_j^T \, \mathbf{A}_E \, \mathbf{B}_i = \mathbf{B}_j^T \, \mathbf{R}_i = 0$. □

The lemma implies that the (i,k)-entry of matrix $\hat{\mathbf{A}}_E^1$ is the dot-product $\mathbf{B}_i^T\,\mathbf{R}_k$; therefore, this matrix can be calculated easily.

Remark 3.1. *Analysis of diffusion equations [11] reveals that the accuracy requirement (the right formula in (4)) alone is not sufficient to build a convergent numerical scheme for operator (2). What is needed are the orthogonality conditions (6) and the relations between vectors* $\mathbf{R}_i$ *and* $\mathbf{B}_i$*. The latter are related to existence of special discrete Gauss-Green relations on element E.*

We define m basis vectors $\mathbf{B}_i$ using the degrees of freedom of linear vector-functions $\boldsymbol{\psi}_i$. Recall that the entries of $\mathbf{B}_i$ are the values of $\boldsymbol{\psi}_i$ at vertices of polyhedron E. In three-dimensions, there are twelve linearly independent linear vector-functions, which gives $m = 12$. In two-dimensions, $m = 6$. To define the vectors $\mathbf{R}_i$ corresponding to the selected basis vectors, we take the second formula in (4) and replace the tensor μ by a constant tensor μ_E. This is the order of h approximation. Then, replacing $\mathbf{u}$ by $\boldsymbol{\psi}_i$ and integrating by parts, we get

$$\begin{aligned} |E|\,O(h) + \mathbf{B}_i^T\,\mathbf{A}_E\,\mathbf{V}_E &= \int_E (\mu_E \nabla\boldsymbol{\psi}_i) : \nabla\mathbf{v}\,\mathrm{d}V \\ &= -\int_E \mathrm{div}\,(\mu_E\nabla\boldsymbol{\psi}_i)\cdot\mathbf{v}\,\mathrm{d}V + \int_{\partial E}((\mu_E\nabla\boldsymbol{\psi}_i)\cdot\mathbf{n}_E)\cdot\mathbf{v}\,\mathrm{d}S \\ &= \sum_{f\in\partial E}((\mu_E\nabla\boldsymbol{\psi}_i)\cdot\mathbf{n}_E)\cdot\int_f \mathbf{v}\,\mathrm{d}S. \end{aligned} \tag{7}$$

The last integral over face f can be approximated using the degrees of freedom of $\mathbf{v}$ at vertices of f. Let $\mathbf{x}_f$ be the center of gravity of face f. There exist positive coefficients $\omega_{f,v}$ such that

$$\mathbf{x}_f = \sum_{v\in f}\omega_{f,v}\mathbf{x}_v.$$

Using this formula in (7), we get

$$|E|\,O(h) + \mathbf{B}_i^T\,\mathbf{A}_E\,\mathbf{V}_E = \sum_{f\in\partial E}((\mu_E\nabla\boldsymbol{\psi}_i)\cdot\mathbf{n}_E)\cdot\sum_{v\in f}\omega_{f,v}\mathbf{V}_{E,v} + |E|\,O(h).$$

Finally, neglecting the $O(h)$ terms and re-arranging the terms in the right-hand side, we obtain the following discrete Gauss-Green relations:

$$\mathbf{B}_i^T\,\mathbf{A}_E\,\mathbf{V}_E = ((\mu_E\nabla\boldsymbol{\psi}_i)\cdot\mathbf{n}_E)\cdot\sum_{v\in f}\omega_{f,v}\mathbf{V}_{E,v} \equiv \mathbf{R}_i^T\,\mathbf{V}_E. \tag{8}$$

Due to arbitrariness of $\mathbf{V}_E$, we derive the desired relations $\mathbf{A}_E\,\mathbf{B}_i = \mathbf{R}_i$ *without knowledge of the matrix* $\mathbf{A}_E$. It is pertinent to note that the above derivations hold for arbitrary polyhedron E. This polyhedron may be non-convex and degenerate.

No information is available to specify the matrix $\hat{\mathbf{A}}_E^2$; thus, it remains arbitrary. For a hexahedral element, this is the matrix of size six. At the moment it is not clear how to use this flexibility to obtain additional properties from the final scheme. In practice, we use a diagonal matrix, $\hat{\mathbf{A}}_E^2 = \alpha_E\mathbf{I}_E$. A reasonable choice for the scaling parameter α_E is the mean trace of the first diagonal block, $\alpha_E = \mathrm{trace}(\hat{\mathbf{A}}_E^1)/m$.

Lemma 3.2. *Let E be a tetrahedron and* μ *be a constant tensor. Then, the matrix* $\mathbf{A}_E$ *coincides with the finite element matrix for linear finite elements.*

Proof. For a tetrahedron, $m = n_{E,v} = 12$. Thus, no room is left for the matrix $\hat{\mathbf{A}}_E^2$. Note that the finite element functions on E are linearly independent functions. Selecting $\boldsymbol{\psi}_i$ as the finite element functions, we get that $\mathbf{B}_E$ is the identity matrix and the (i,k)-th entry of $\hat{\mathbf{A}}_E^1$ is

$$(\hat{\mathbf{A}}_E^1)_{i,k} = \mathbf{B}_i^T\mathbf{R}_k = \int_E (\mu_E\nabla\boldsymbol{\psi}_i) : \nabla\boldsymbol{\psi}_k\,\mathrm{d}V.$$

Thus, $\hat{\mathbf{A}}_E^1$ is the finite element stiffness matrix. The proof is completed by noting that this matrix coincides with $\hat{\mathbf{A}}_E$. □

4. Numerical experiments

The method derived above allows μ_E to be the fourth-order tensor. This flexibility is not yet used in the presented numerical experiments. More precisely, we use the following expression for the scalar viscosity coefficient μ_E [13]:

$$\mu_E = \chi_E \rho_E L_E \left(c_Q \frac{\gamma+1}{4} |\Delta u| + \sqrt{c_Q^2 \left(\frac{\gamma+1}{4}\right)^2 |\Delta u|^2 + c_L^2 s_E^2} \right),$$

where s_E is the sound speed, c_L and c_Q are positive non-dimensional constants, L_E is the characteristic length, Δu is the measure of compressibility (a scalar, for instance, the velocity jump across the shock), and χ_E is a binary switch.

The binary switch ensures that the heating due to artificial viscosity occurs only for elements under compression. We set $\chi_E = 0$ when $\Delta u > 0$ and $\chi_E = 1$ otherwise. The measure of compression is defined as the mean divergence of the velocity multiplied by the characteristic length.

In the numerical experiments, we set $c_L = c_Q = 1$. We use a simple estimates for the characteristic length L_E, $L_E = \sqrt[3]{|E|}$. This estimate is appropriate for meshes with mild variation of volumes of neighboring elements.

The TAV does not control hourglass distortion of the mesh. Therefore, additional numerical viscosity is added to the discrete momentum equation using the temporal triangular subzoning (TTS) method [14]. We verified with numerical experiments that both viscosities are required in the simulations described below.

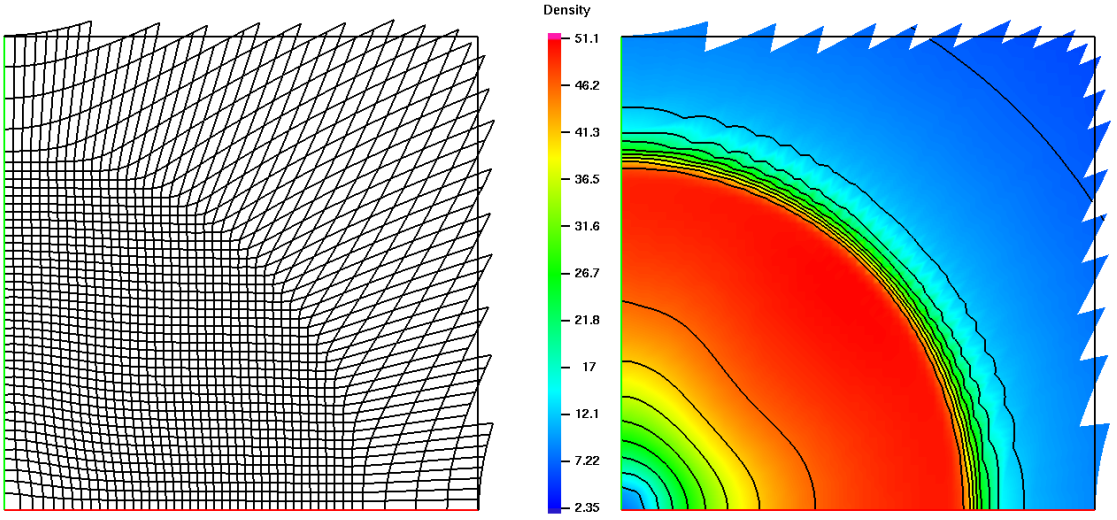

Figure 1: The three-dimensional Noh implosion problem in the $r-z$ coordinate system. Left picture shows the logically square mesh at time $t = 0.6$. Part of the mesh ahead of the shock has been removed for visualization clarity. Right picture shows density isolines.

The simulations were done using the code [2]. In the first experiment, we consider the three-dimensional Noh implosion problem [15], where the ideal gas with $\gamma = 5/3$, density $\rho = 1.0$, and pressure $p = 0$ is given an initial unit inwards radial velocity. A spherical shock wave is generated at the origin and moves with constant speed $1/3$. At time $t = 0.6$, the shock wave has radial coordinate 0.2. The density behind shock is 64.

Using symmetry of the problem, we may solve it in two-dimensions. Results of the two-dimensional experiment are shown in Fig. 1. The initial computational mesh is the 50×50 square mesh occupying the unit square. The final mesh at time $t = 0.6$ has high-quality quadrilateral elements. The gas heating near the origin is the well known intrinsic feature of Lagrangian simulations. The density isolines indicates acceptable preservation of cylindrical symmetry. On the top-left picture in Fig. 2, we plot density at centroids $\mathbf{x}_E$, $E \in \mathcal{T}_h$, versus the distance to the origin. Around the shock, we observe approximately 5% variation of density in the angular direction.

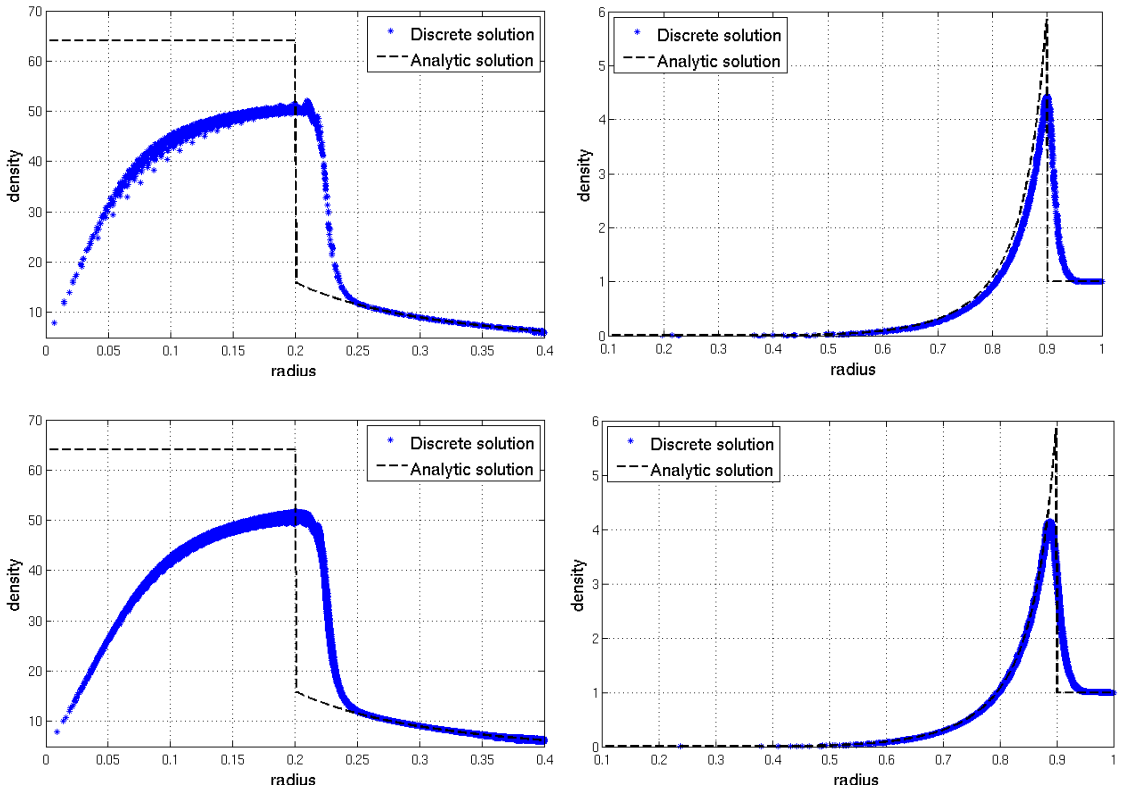

Figure 2: The density at centroids of mesh elements (stars) versus the distance to the origin for the Noh (left column) and Sedov (right column) problems. The top row shows results of two-dimensional simulations that exploit spherical symmetry of the problems. The bottom row shows results of three-dimensional simulations.

Now, the same problem is solved in three-dimensions. The initial mesh is the $40 \times 50 \times 60$ orthogonal mesh. The trace of the final mesh at time $t = 0.6$ is shown in Fig. 3. We observe a high quality logically cubic mesh. We also observe that the density behind the shock is smaller than the theoretical value of 64 but is approximately the same as in the two-dimensional simulation. This may be related to the isotropic nature of the scalar viscosity coefficient μ. Finally, we note that violation of spherical symmetry is bounded again by 5%.

In the second experiment, we consider the Sedov explosion problem. The problem generates a strong diverging shock wave [16, 17]. The initial density of the ideal gas with $\gamma = 1.4$ is unity and the initial velocity is zero. At $t = 0$, the total energy E_0 is all internal and concentrated at the origin. The analytical solution gives the expanding shock of radius r_s with peak density of 6,

$$r_s = \left(\frac{E_0 \, t^2}{\alpha_s \, \rho_0} \right)^{0.2},$$

where $\alpha_3 = 0.850937$. The total energy E_0 is defined such that $r_s = 0.9$ at time $t = 1$.

We consider a 50×50 square mesh occupying initially the unit square. Only one element near the origin (the biggest element in Fig. 4) is given a non-zero specific internal energy. The mesh elements are compressed in the radial direction and have large obtuse angles. Note that only small angles (close to 0°) may reduce (theoretically) the accuracy of the mimetic discretization. The right picture in Fig. 4 and the top-right picture in Fig. 2 show small variation of density in the angular direction.

The same problem is solved in three-dimensions. The initial mesh is the $48 \times 48 \times 48$ orthogonal mesh. The trace of the final mesh at $t = 1$ is shown in Fig. 5. All hexahedra have high quality according to the mesh criteria formulated

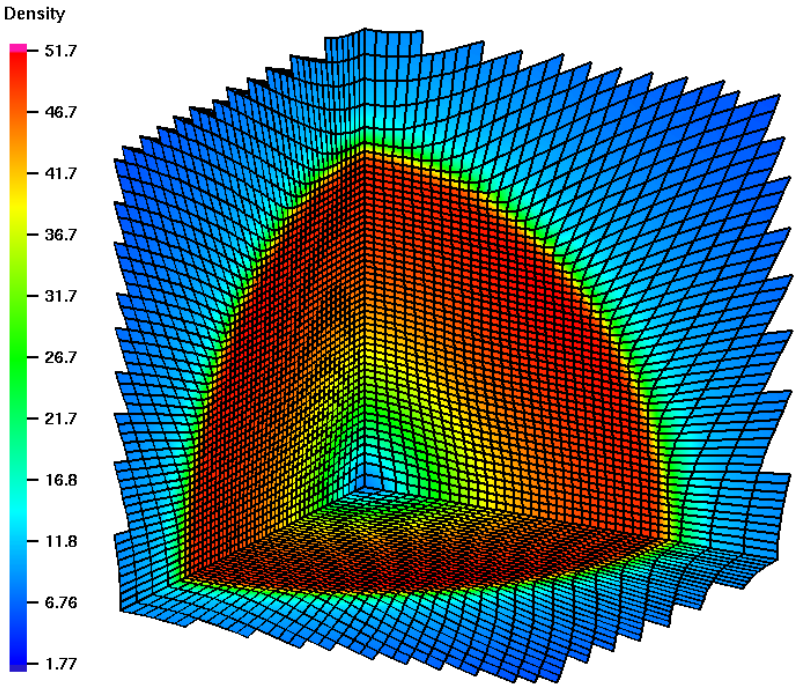

Figure 3: The three-dimensional Noh implosion problem on a logically cubic mesh. The mesh trace is shown on three sides of the computational domain that are attached to the origin. Part of the mesh ahead of the shock has been removed for visualization clarity. The colors show density distribution.

in [11] for polyhedral meshes. We recall that presence of large obtuse dihedral angles does not necessary affect the mesh quality. In the bottom-right picture in Fig. 2, we observe slight reduction of the pike density compared to the two-dimensional simulation (the top-right picture). On the other hand, position of the shock is more accurate in the three-dimensional simulation.

5. Conclusion and future work

We derived a new mimetic tensor artificial viscosity on general polyhedral meshes. The tensor viscosity is designed as the mimetic discretization of the differential operator $\mathrm{div}\,(\mu\nabla\mathbf{u})$, where μ is the full fourth-order tensor. We demonstrated performance of the new viscosity with a few two-dimensional and three-dimensional Lagrangian simulations.

In the future, we plan to develop and analyze tensorial viscosity coefficients μ. This will help to reduce dissipation in directions transverse to the shock direction.

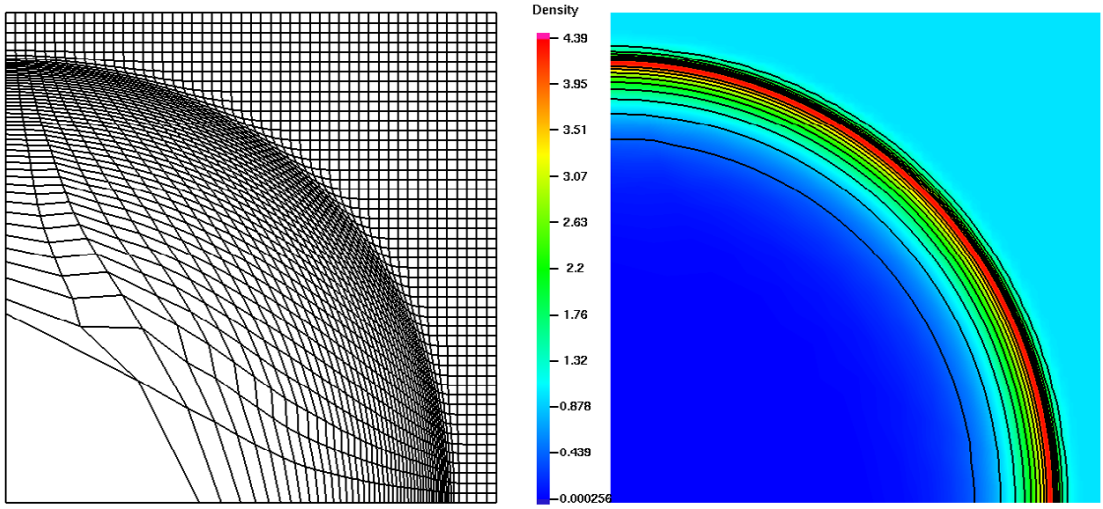

Figure 4: The three-dimensional Sedov explosion problem in the r-z coordinate system. Left picture shows the logically square mesh a time $t = 1$. Right picture shows density isolines.

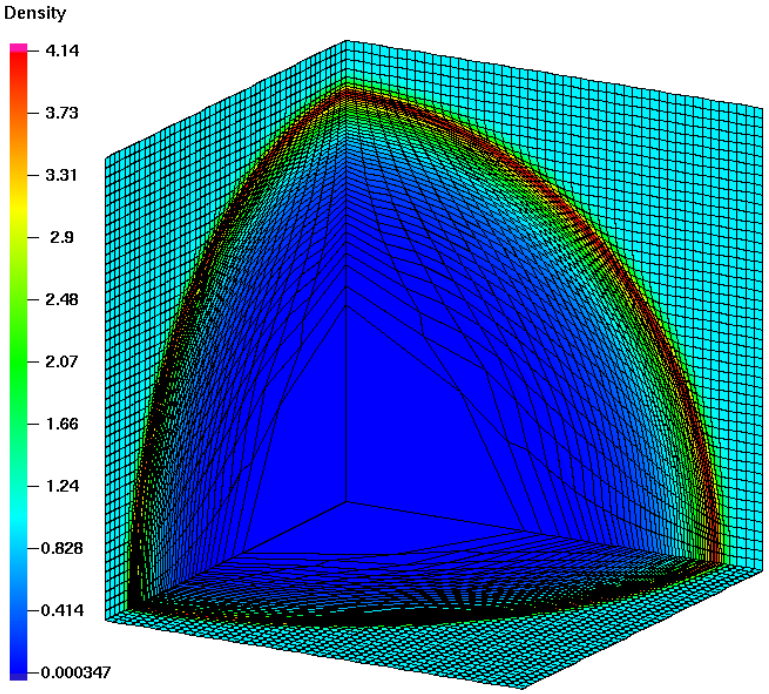

Figure 5: The three-dimensional Sedov explosion problem on a logically cubic mesh. The mesh trace is shown on three sides of the computational domain that are attached to the origin (the vertex of the biggest element). The colors show density distribution.

References

[1] Z. Warsi. *Fluid Dynamics. Theoretical and Computational Approaches*. CRC Press, Boca Raton, 1993.
[2] D. E. Burton. Consistent finite-volume discretization of hydrodynamics conservation laws for unstructured grids. Technical report UCRL-JC-118788, Lawrence Livermore National Laboratory, 1994.
[3] J. von Neumann, and R.D. Richtmyer. A method for calculation of hydrodynamic shocks. *J. Appl. Phys.* (1950) **21**, 232-237.
[4] W.D. Schulz. Tensor artificial viscosity for numerical hydrodynamics. *J. Math. Phys.* (1964) **5**, 133-138.
[5] R. Landshoff. A numerical method for treating fluid flow in the presence of shocks. Technical report LA-1930, Los Alamos National Laboratory, 1955.
[6] E. Caramana, M. Shashkov, and P. Whalen. Formulation of artificial viscosity for multi-dimensional shock wave calculations. *J. Comput. Phys.* (1998) **144**, 70–97.
[7] K. Lipnikov, and M. Shashkov. A mimetic tensor artificial viscosity on arbitrary polygonal meshes. Technical report LA-UR-10-00006, Los Alamos National Laboratory, 2010.
[8] J. Campbell and M. Shashkov. A tensor artificial viscosity using a mimetic finite difference algorithm. *J. Comput. Phys.* (2001) **172**, 739–765.
[9] T. Kolev and R. Rieben. A tensor artificial viscosity using a finite element approach. *J. Comput. Phys.* (2009) **228**:22, 8336–8366.
[10] M. Berndt, and K. Lipnikov, and J.D. Moulton, and M. Shashkov. Convergence of mimetic finite difference discretizations of the diffusion equation. *East-West J. Numer. Math.* (2001) **9**, 253–284.
[11] F. Brezzi, K. Lipnikov, and V. Simoncini. A family of mimetic finite difference methods on polygonal and polyhedral meshes. *Math. Models Methods Appl. Sci.* (2005) **15**:10, 1533–1551.
[12] F. Brezzi, A. Buffa, and K. Lipnikov. Mimetic finite differences for elliptic problems. *M2AN Math. Model. Numer. Anal.* (2009) **43**, 277–295.
[13] M. Wilkins. Use of artificial viscosity in multidimensional shock wave problems. *J. Comput. Phys.* (1980) **36**, 281–303.
[14] P. Browne and K. Wallick. The reduction of mesh tangling in two-dimensional Lagrangian hydrodynamics codes by the use of viscosity, artificial viscosity, and TTS (temporary triangular subzoning for long, thin zones). Technical report LA-470-MS, Los Alamos National Laboratory, 1971.
[15] W. Noh. Errors for calculations of strong shocks using an artificial viscosity and an artificial heat flux. *J. Comput. Phys.* (1987) **72**, 78–120.
[16] L. Sedov. *Similarity and Dimensional methods in mechanics*. Academic Press, New York, 1959.
[17] A. Shestakov. Time-dependent simulations of point explosion with heat conduction. *Physics of Fluids* (1999), **11**, 1091–1095.